

LETTER • OPEN ACCESS

## Large sub-regional differences of ammonia seasonal patterns over India reveal inventory discrepancies

To cite this article: Christopher A Beale *et al* 2022 *Environ. Res. Lett.* **17** 104006

View the [article online](#) for updates and enhancements.

You may also like

- [Global, regional and national trends of atmospheric ammonia derived from a decadal \(2008–2018\) satellite record](#)  
Martin Van Damme, Lieven Clarisse, Bruno Franco et al.
- [Tropospheric ozone data assimilation in the NASA GEOS Composition Forecast modeling system \(GEOS-CF v2.0\) using satellite data for ozone vertical profiles \(MLS\), total ozone columns \(OMI\), and thermal infrared radiances \(AIRS, IASI\)](#)  
Makoto M Kelp, Christoph A Keller, Krzysztof Wargan et al.
- [Atmospheric summer teleconnections and Greenland Ice Sheet surface mass variations: insights from MERRA-2](#)  
Young-Kwon Lim, Siegfried D Schubert, Sophie M J Nowicki et al.



The Breath Biopsy® Guide  
Fourth edition

FREE

DOWNLOAD THE FREE E-BOOK

BREATH BIOPSY

OWLSTONE MEDICAL

ENVIRONMENTAL RESEARCH  
LETTERS

## LETTER

## Large sub-regional differences of ammonia seasonal patterns over India reveal inventory discrepancies

## OPEN ACCESS

## RECEIVED

15 September 2021

## REVISED

1 August 2022

## ACCEPTED FOR PUBLICATION

9 August 2022

## PUBLISHED

16 September 2022

Original content from this work may be used under the terms of the [Creative Commons Attribution 4.0 licence](#).

Any further distribution of this work must maintain attribution to the author(s) and the title of the work, journal citation and DOI.



Christopher A Beale<sup>1</sup>, Fabien Paulot<sup>2</sup>, Cynthia A Randles<sup>3</sup>, Rui Wang<sup>1</sup> , Xuehui Guo<sup>1</sup>, Lieven Clarisse<sup>4</sup>, Martin Van Damme<sup>4</sup>, Pierre-François Coheur<sup>4</sup>, Cathy Clerbaux<sup>4,5</sup>, Mark W Shephard<sup>6</sup> , Enrico Dammers<sup>6</sup>, Karen Cady-Pereira<sup>7</sup> and Mark A Zondlo<sup>1,\*,\*\*</sup> 

<sup>1</sup> Civil and Environment Engineering, Princeton University, Princeton, NJ, United States of America

<sup>2</sup> Geophysical Fluid Dynamics Laboratory, NOAA, Princeton, NJ, United States of America

<sup>3</sup> ExxonMobil Technology and Engineering Company, Annandale, NJ, United States of America

<sup>4</sup> Université libre de Bruxelles (ULB), Spectroscopy, Quantum Chemistry and Atmospheric Remote Sensing (SQUARES), Brussels, Belgium

<sup>5</sup> LATMOS/IPSL, Sorbonne Université, UVSQ, CNRS, Paris, France

<sup>6</sup> Environment and Climate Change Canada, Toronto, Ontario, Canada

<sup>7</sup> Atmospheric and Environmental Research (AER), Lexington, MA, United States of America

\* Now at UNEP International Methane Emissions Observatory.

\*\* Author to whom any correspondence should be addressed.

E-mail: [mzondlo@princeton.edu](mailto:mzondlo@princeton.edu)

**Keywords:** India, biomass burning, agriculture, emissions, ammonia, air quality, satellite

Supplementary material for this article is available [online](#)

**Abstract**

Ammonia (NH<sub>3</sub>) is a key precursor of haze particles and fine particulate matter (PM<sub>2.5</sub>) and its spatiotemporal variabilities are poorly constrained. In this study, we present measurements of NH<sub>3</sub> over the Indian subcontinent region from the Infrared Atmospheric Sounder Interferometer (IASI) and Cross-track Infrared Sounder (CrIS) satellite instruments. This region exhibits a complex emission profile due to the number of varied sources, including crop burning, fossil fuel combustion, fertilizer application, livestock and industrial sources. Observations from the CrIS and IASI instruments are oversampled to a resolution of 0.02° × 0.02°. Five regions with distinct spatiotemporal NH<sub>3</sub> profiles are determined using k-means clustering. Maximum NH<sub>3</sub> columns are seen in July over the western India with column densities of 6.2 × 10<sup>17</sup> mol cm<sup>-2</sup> and 7.2 × 10<sup>17</sup> mol cm<sup>-2</sup> respectively for IASI and CrIS. The seasonality of measured NH<sub>3</sub> columns show annual maxima occurring in spring in Eastern India and Bangladesh and in mid-summer for the western Indo-Gangetic plain. Our observational constraints suggest that the impact of local farming practices on NH<sub>3</sub> emissions is not well captured in emission inventories such as Coupled Model Intercomparison Project Phase 6 (CMIP6), which exhibits peaks in the late spring and autumn. The spatial variability in the seasonal patterns of NH<sub>3</sub> is also not captured by the single emissions profile used in CMIP6 for India. The high-resolution maps obtained from these measurements can be used to improve NH<sub>3</sub> emission inventories in order to understand its sources for more accurate predictions of air quality in the Indian subcontinent. Our study points to the need for regionally specific emissions inventories for short-lived species such as NH<sub>3</sub> that have heterogeneous emissions profiles due to specific agricultural practices and other emission source characteristics.

**1. Introduction**

Ammonia (NH<sub>3</sub>) is a major component of the global nitrogen cycle and the most abundant alkaline gas in the atmosphere (Mosquera *et al* 2005, Sutton *et al* 2020). It plays a major role in the formation

of atmospheric aerosols (Pan *et al* 2016) and is a key precursor to fine particulate matter (PM) (Gong *et al* 2013). Deposition of NH<sub>3</sub> into ecosystems can lead to eutrophication and acidification of the soils and waterways leading to decreased biodiversity (Leip *et al* 2015). NH<sub>3</sub> has a short lifetime of

0.5–5 days (Walker *et al* 2000) and exhibits a highly heterogeneous spatial distribution. Ammonia readily reacts with atmospheric acids, particularly nitric acid and sulfuric acid to form ammonium nitrate and ammonium sulfate respectively (Adams *et al* 1999). The short lifetime of  $\text{NH}_3$  and the dependence of both formation and sinks on climatic conditions, such as atmospheric temperature and humidity, results in large uncertainties on both emissions and atmospheric concentrations (Hellsten *et al* 2018).

India experiences some of the worst air pollution in the world (World Health Organization 2016), and air quality concerns extend throughout much of the continent (Hammer *et al* 2020, Ravishankara *et al* 2020). Ammoniated aerosols over the Indian subcontinent are significant components of unhealthy PM (Kumar and Sarin 2010, Sudheer and Rengarajan 2015, Saraswati *et al* 2019, Ojha *et al* 2020, Acharja *et al* 2022). The Indo-Gangetic Plain (IGP) is a highly polluted area consisting of parts of Pakistan, northern India, southern Nepal and most of Bangladesh. Sources of aerosols in this region include biomass burning (including waste), vehicular emissions, industrial activity and desert dust (Singh *et al* 2017). In particular, the IGP is a major emissions hotspot for  $\text{NH}_3$  (Parashar *et al* 1998, Clarisse *et al* 2009, Van Damme *et al* 2018). The region shows strong seasonal variability in PM (Awasthi *et al* 2011, Mahapatra *et al* 2018) due to unique meteorology, orography and seasonal emissions, such as crop burning. Crop clearance via burning is especially common in India (Jain *et al* 2014) where plant residues from common crops, such as wheat, barley and rice, are removed.

Although  $\text{NH}_3$  is critical in the formation of PM and atmospheric aerosols, anthropogenic emissions are not widely regulated (Felix *et al* 2017, Sharma *et al* 2020) and  $\text{NH}_3$  is not considered a criteria pollutant in the United States (Gilliam and Hall 2016), though is regulated in the European Union. The Central Pollution Control Board of India has a limited number of  $\text{NH}_3$  sensors in its network (Pant *et al* 2019) and additional surface concentrations have been measured at the local scale, particularly in Delhi (Saraswati *et al* 2018, Kotnala *et al* 2020). As a result, there is limited spatial coverage in this region and specifically a lack of long-term surface measurements.

Current available emissions inventories, both global and local, do not have sufficiently accurate  $\text{NH}_3$  emissions for the Indian subcontinent for use with atmospheric models.  $\text{NH}_3$  readily reacts with sulfuric acid and nitric acid, leading to the formation of ammonium sulfate and ammonium nitrate. The proportion of  $\text{PM}_{2.5}$  made up of these secondary inorganic aerosols varies by region and season (Park *et al* 2021), mainly due to the strong dependence on temperature of ammonium nitrate formation (Pinder *et al* 2008). In order for atmospheric models to accurately predict the distribution of PM in India,

more appropriate regional emissions inventories are required.

Improvements in satellite instruments and retrieval algorithms have enabled measurement of atmospheric  $\text{NH}_3$  from space. Satellite remote sensing of atmospheric gases allows measurements with spatial coverage beyond that available from ground-based measurements. The first satellite measurements of lower tropospheric  $\text{NH}_3$  were achieved with the Tropospheric Emission Spectrometer (TES) (Beer *et al* 2008, Shephard *et al* 2011) and subsequently the Infrared Atmospheric Sounder Interferometer (IASI) (Clarisse *et al* 2009), the Cross-track Infrared Sounder (CrIS) (Shephard and Cady-Pereira 2015), the Atmospheric Infrared Sounder (AIRS) (Warner *et al* 2017), and Greenhouse Gases Observing Satellite (Someya *et al* 2020) have added to the suite of instruments measuring  $\text{NH}_3$  from space. Satellite remote sensing has previously been used to study  $\text{NH}_3$  in India, including annual trends (Van Damme *et al* 2021). Spatiotemporal analyses have also been carried out over India, including the IGP, on a monthly basis at IASI native resolution (Kuttippurath *et al* 2020) and at coarser resolutions for comparison with models (Pawar *et al* 2021). These analyses use pre-existing political or geographical boundaries to study regional trends.

The work presented here follows a data-driven approach to determine distinct regions of  $\text{NH}_3$  seasonality at high resolution achieved from oversampling many years of data from two independent satellite platforms, IASI and CrIS. The purpose of this study is to use satellite remote sensing to measure the spatiotemporal distribution of  $\text{NH}_3$  in the Indian subcontinent and explore sub-regions where further, particularly bottom up, studies should be focused. Using the multi-year  $\text{NH}_3$  products from the IASI and CrIS instruments we present spatial and seasonal variations in  $\text{NH}_3$  columns over India, Pakistan and Bangladesh. In support of using IASI and CrIS measurements, a detailed analysis of the  $\text{NH}_3$  seasonal cycle over France was performed using both IASI and CrIS (Viatte *et al* 2020), and IASI and CrIS showed similar spatiotemporal  $\text{NH}_3$  patterns despite different overpass times, instruments and retrieval algorithms. A *k*-means clustering technique is employed on the oversampled satellite data to classify regions with approximately similar seasonality in this study area based on monthly means.

## 2. Method

The IASI instrument measures the N–H stretching mode of  $\text{NH}_3$  at around  $950\text{ cm}^{-1}$  (Coheur *et al* 2009). Three such instruments are in orbit on the Metop-A, -B and -C satellites in sun-synchronous orbits, each having two overpasses per day at a local time of approximately 0930 and 2130. As a result, IASI achieves global coverage two times per day with pixel

size  $12 \text{ km} \times 12 \text{ km}$  at nadir (up to  $20 \text{ km} \times 39 \text{ km}$  at the edge of the swath) and a swath width of 2400 km. As thermal contrast is an important factor in instrument sensitivity and therefore retrieval quality, only the measurements from the morning overpasses of Metop-A and -B were used for this study due to limited thermal contrast for the nighttime overpasses. Measurements with more than 10% cloud contamination were not included. Version 3 of the IASI  $\text{NH}_3$  retrievals have been used for this analysis for the years 2008–2017 (Franco *et al* 2018, Van Damme *et al* 2021).

CrIS is a Fourier Transform spectrometer deployed on board the Suomi-NPP satellite, launched on October 2011. Suomi-NPP is in a sun-synchronous orbit with two overpasses per day at approximately 0130 and 1330, providing global coverage with a swath width of approximately 2200 km. Only measurements from the ascending node in the afternoon have been considered here. The instrument has a high spectral resolution of  $0.625 \text{ cm}^{-1}$  (Tobin *et al* 2013) and circular  $3 \times 3$  pixels, with a 14 km diameter at nadir. CrIS has a similar spatial coverage to IASI (Shephard and Cady-Pereira 2015) but has decreased spectral noise in the  $950 \text{ cm}^{-1}$  spectral region (Zavvalov *et al* 2013). The detection limit of CrIS is approximately 0.9 ppbv (Shephard and Cady-Pereira 2015) and can reach down to 0.3 ppbv under ideal conditions (Kharol *et al* 2018). The CrIS product version 1.5 data were used for this analysis for the period 2013–2017 (Shephard *et al* 2020).

Direct validation of satellite remote sensed  $\text{NH}_3$  has been conducted by ground-based or aircraft measurements. For IASI, such validation has been performed in the USA (Guo *et al* 2021) and Europe, China and Africa (Van Damme *et al* 2015; Dammers *et al* 2016). For CrIS, ground-based fourier transform infrared spectroscopy (FTIR) has been used in sites in North America, Europe and Oceania (Dammers *et al* 2017).

An oversampling algorithm (Sun *et al* 2018, Van Damme *et al* 2018) was used to spatially and temporally average both datasets to a  $0.02 \times 0.02^\circ$  grid over the region  $5\text{--}40^\circ \text{ N}$  and  $65\text{--}100^\circ \text{ E}$ , covering the total area of India and Bangladesh and most of Pakistan. This method of spatial averaging leads to higher resolution and fewer gaps between observations at the price of temporal resolution. For this analysis, monthly averages for the entire ten and five year IASI and CrIS datasets, respectively, were considered, and inter-annual variability was not taken into account.

An iterative  $k$ -means clustering approach was used to analyze the spatiotemporal variability of  $\text{NH}_3$  columns in the study region.  $k$ -means clustering techniques have been used for a number of geophysical applications to classify datasets (Wang *et al* 2021).

This  $k$ -means approach groups data into clusters whereby the averaged squared distance between data within a cluster are minimized (Forgy 1965, Arthur

and Vassilvitskii 2007). Thus, no prior assumed regions, such as political or geographical boundaries, are used to determine regionality of data, rather the clustering is driven by the data itself and minimizes instrument bias. This is particularly important for low column measurements.

Firstly, monthly  $\text{NH}_3$  data were standardized to have a mean of 0 and a variance of 1 to avoid observations being grouped by magnitude or differences in mean or variance. The approach then uses  $k$  pre-defined centroids and allocates each value in the set ( $z_n$ ) based on reducing the sum of squares of each cluster ( $C$ ), so as to minimize  $J$  where,

$$J = \sum_{i=1}^k \sum_{z_n \in C_i} (z_n - \bar{z}_i)^2.$$

First, 20 seeds were randomly selected (land only) for clustering (i.e.  $k = 20$ ) and the seasonality of each pixel in the study was compared to each of the seeds and allocated based on minimizing  $J$ . When each pixel had been classified to a cluster, the pixels in each cluster were averaged to calculate a new seed value. This process was iterated until convergence, where clusters did not change upon iteration. One issue with a  $k$ -means clustering approach is the initial selection of the number of seeds. For this study,  $k$  was set to be high (20). At iteration, if a cluster  $C$  contained only one pixel (i.e. it matched only with itself), it was removed for the next iteration. Through this method, the number of clusters ended at five for both IASI and CrIS. This process was repeated 10 000 times to test if selection of random seeds at the second step would affect the result. Though certain seed selections had minor effects (for example mountainous pixels, or those overlapping land and ocean), random seed selection did not significantly change the resulting clusters and therefore their seasonalities.

### 3. Results

The monthly oversampled high-resolution maps of  $\text{NH}_3$  over the study area are presented in figure 1 for IASI and figure 2 for CrIS. A comparison between the  $\text{NH}_3$  column densities of the two instruments is not the intention of this study, although a month-wise comparison is shown in figure S1 and the seasonality correlation is shown in figure S2. In general, the correlation is very strong from October to April and in regions with high column amounts. The correlation is weakest in the summer months, caused by regions of low  $\text{NH}_3$  (southern India) and missing data in the monsoon season. The short lifetime of  $\text{NH}_3$  and the different overpass times of the satellites makes such an assessment difficult and perhaps misleading; however, both independent datasets show the same general spatial and temporal variability of  $\text{NH}_3$  over the region. The average column measurements over the highly polluted

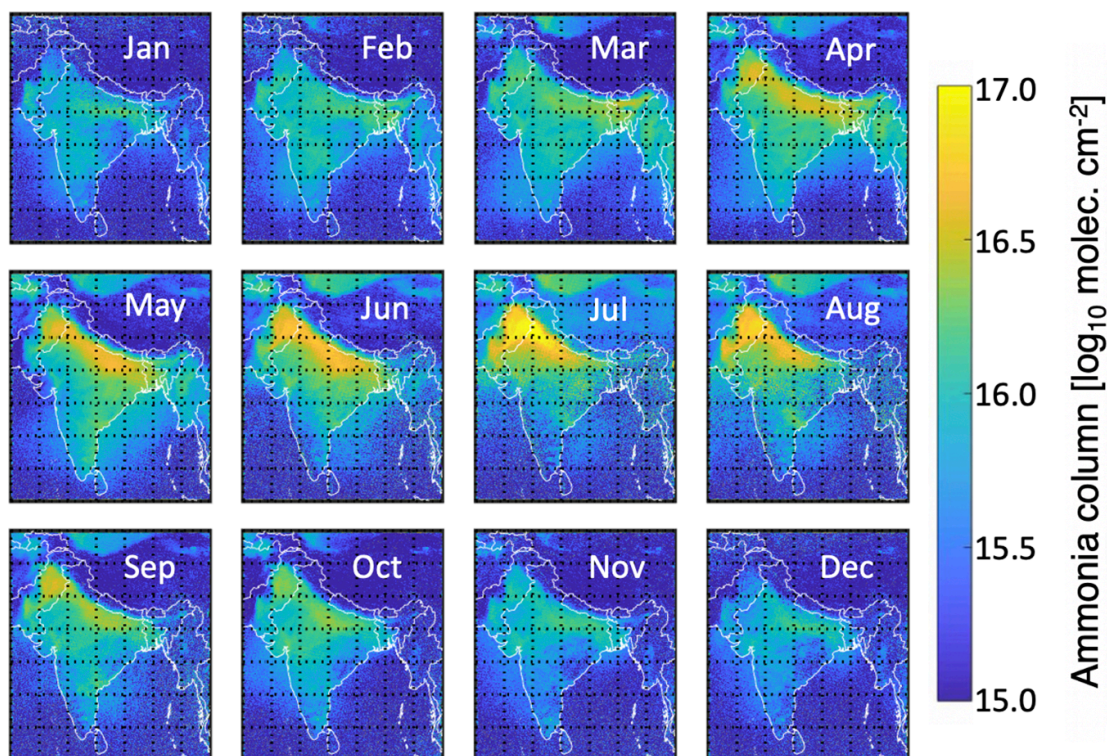


**Figure 1.** IASI monthly average  $\text{NH}_3$  columns (2008–2017) over the Indian subcontinent oversampled at  $0.02^\circ \times 0.02^\circ$  showing the large spatiotemporal variabilities.

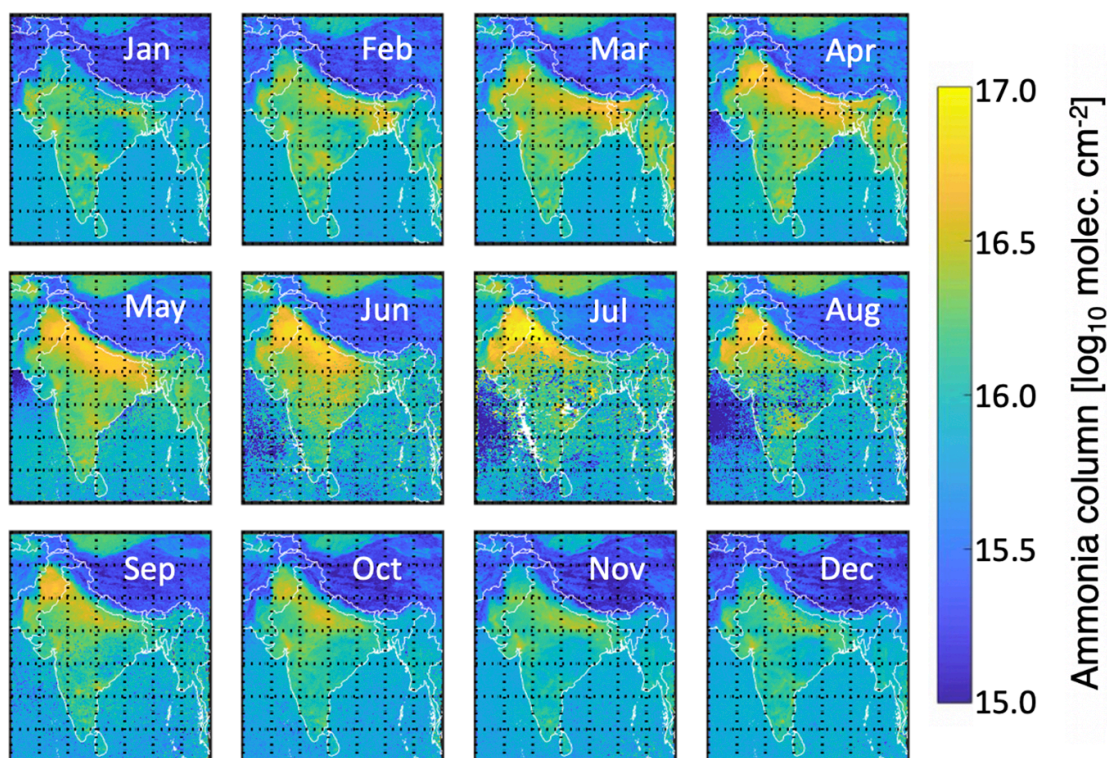
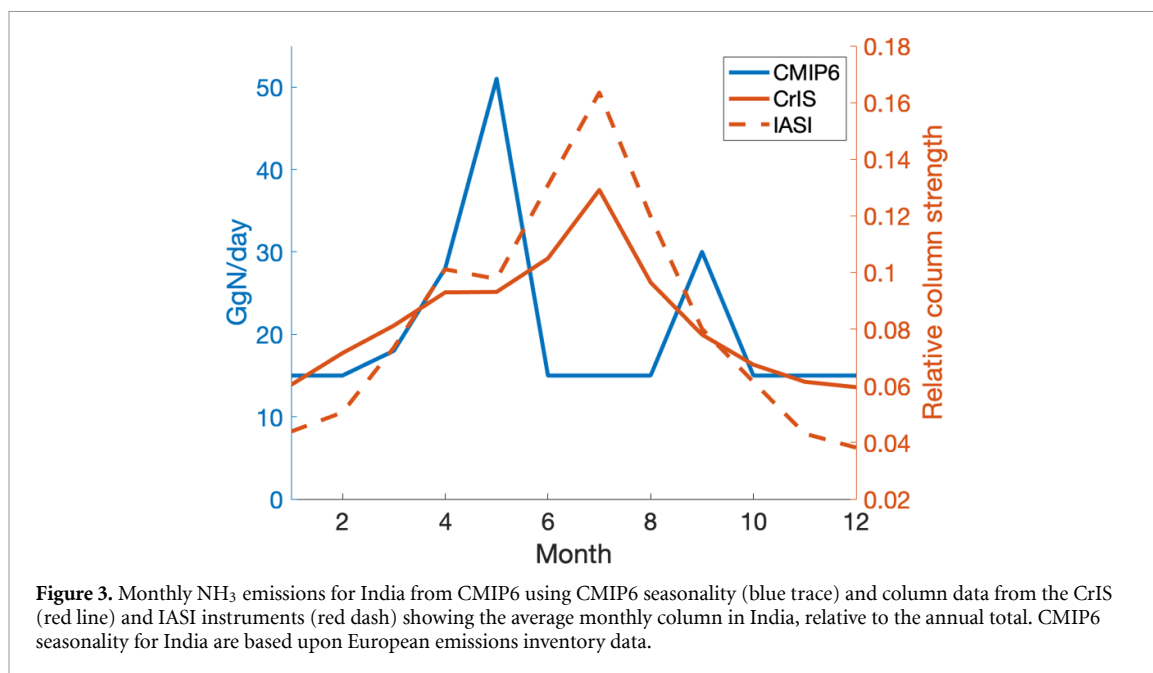


**Figure 2.** CrIS monthly average  $\text{NH}_3$  columns (2013–2017) over the Indian subcontinent oversampled at  $0.02^\circ \times 0.02^\circ$  showing the large spatiotemporal variabilities. Although the absolute column amounts differ relative to IASI, the seasonal and spatial patterns are consistent with those of IASI (figure 1). Missing data are shown in white, largely due to monsoon season cloud cover.



area of the western IGP in its maximum during July are  $4.07 \times 10^{16}$  and  $3.94 \times 10^{16}$  molecules  $\text{cm}^{-2}$  and for the eastern IGP in its maximum during April are  $1.76 \times 10^{16}$  and  $1.60 \times 10^{16}$  molecules  $\text{cm}^{-2}$  for IASI and CrIS, respectively. In addition to the overpass time, sensor differences, instrument sensitivities and different retrieval approaches may result in different measured NH<sub>3</sub> columns. However, in general, the agreement in spatiotemporal distribution between the two sensors in this region is strong, similar to IASI/CrIS analyses in France (Viatte *et al* 2020).

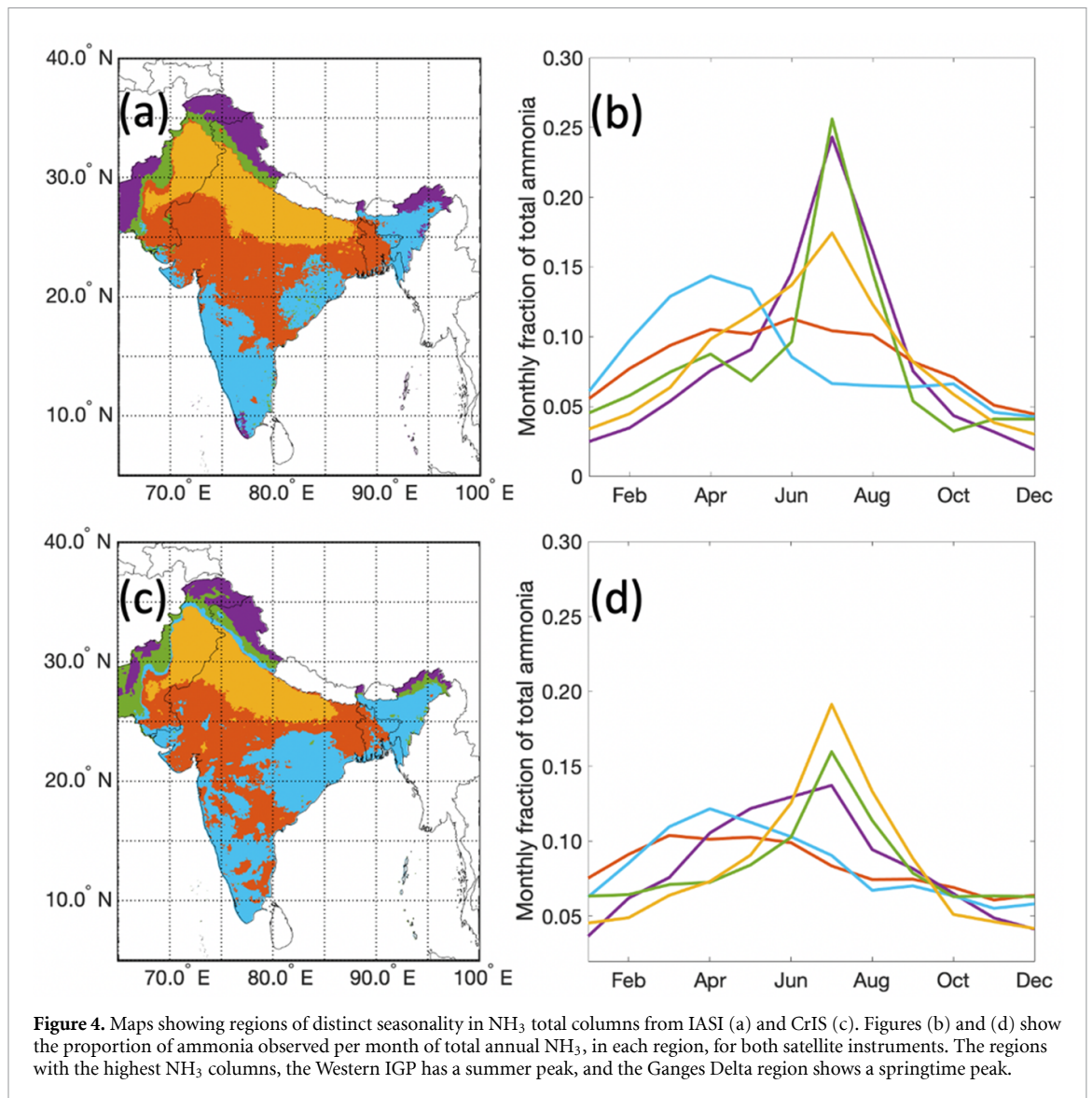
Maximum NH<sub>3</sub> columns are seen in July over the western IGP with column densities of  $6.2 \times 10^{17}$  molecules  $\text{cm}^{-2}$  for IASI and  $7.2 \times 10^{17}$  molecules  $\text{cm}^{-2}$  for CrIS. These results agree spatially with annual average maps of satellite remote sensing of NH<sub>3</sub> over southern Asia (Van Damme *et al* 2014, Kuttippurath *et al* 2020, Someya *et al* 2020). This area is highly populated and contains large areas of intensive agricultural activities including livestock and crop production, most notably, wheat. In contrast, over the eastern IGP, the maximum seasonal columns are in March and April, a local seasonality distinct from the regional average.

Figure 3 demonstrates the large difference between monthly ammonia emissions using the Coupled Model Intercomparison Project Phase 6 (CMIP6) with CrIS and IASI total column measurements. The emissions use seasonality data from the Community Emissions Data System (CEDS) developed for CMIP6 (Hoesly *et al* 2018). The CMIP6 seasonality exhibits a maximum in May and a smaller peak in September. In contrast, satellite observations show that NH<sub>3</sub> column peaks in July, consistent with emissions calculated based on seasonality from observations from AIRS and TES (Warner *et al* 2017,

Paulot *et al* 2018). The larger range of IASI (higher columns in summer and lower in winter, relative to CrIS) result in lower winter contributions to total annual column averages relative to CrIS (and conversely, higher summer contributions). Satellite data from figure 3 show a more accurate seasonality for the greater India region than by using an assumed profile from other regions such as Europe. In CEDS, agricultural NH<sub>3</sub> emissions, the dominant source of NH<sub>3</sub> in India, are distributed across months according to the ECLIPSE v5 model following European practices (Friedrich and Reis 2004, Giglio *et al* 2006). The peaks in May and September correspond to fertilizer application before planting and after harvest. Our results show that this approach does not capture Indian emissions well. The large differences in column strengths and emission sources over different parts of this region, combined with satellite biases, make such a regional averaging approach inaccurate, although improved over using European-based parameterizations. To this end, a *k*-means clustering approach, as applied below, reduces the effect of instrument bias and can discern sub-regional seasonality in more detail.

#### 4. Sub-regional seasonality

The high spatial resolution of NH<sub>3</sub> obtained from oversampling extensive satellite datasets have been analyzed to ascertain sub-regional seasonality of NH<sub>3</sub> over India, Pakistan and Bangladesh. Figures 1 and 2 show how the spatial distribution changes on a monthly basis, but the results of the *k*-means clustering analysis in figure 4 more clearly show the different seasonal distributions of NH<sub>3</sub> in South Asia. The maps have been sub-divided into regions which contain pixels with similar seasonality to each other.



**Figure 4.** Maps showing regions of distinct seasonality in  $\text{NH}_3$  total columns from IASI (a) and CrIS (c). Figures (b) and (d) show the proportion of ammonia observed per month of total annual  $\text{NH}_3$ , in each region, for both satellite instruments. The regions with the highest  $\text{NH}_3$  columns, the Western IGP has a summer peak, and the Ganges Delta region shows a springtime peak.

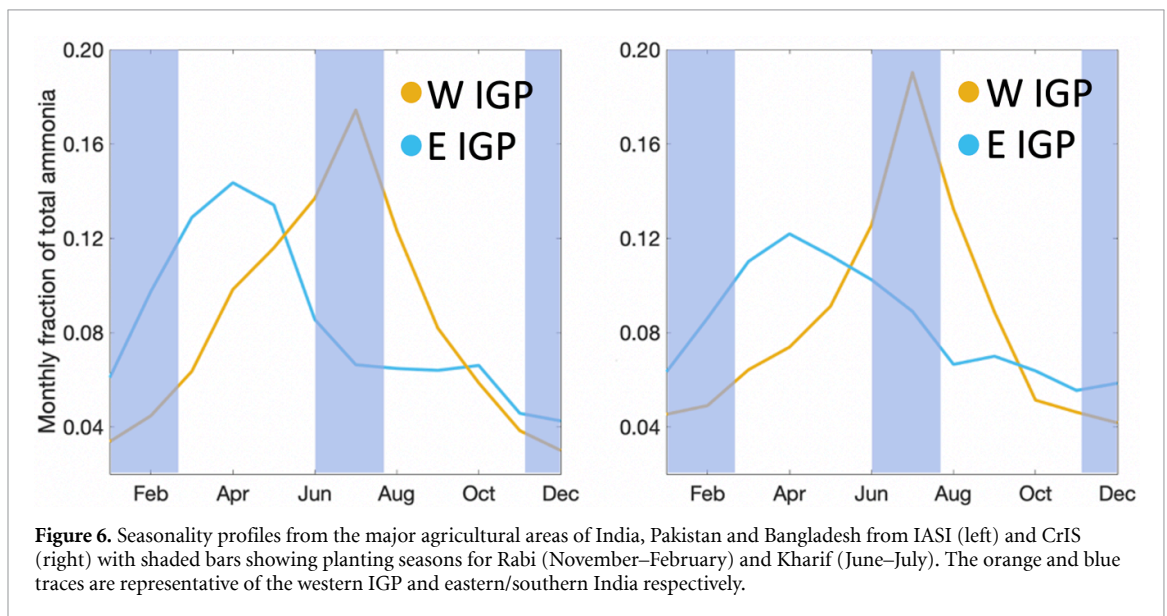
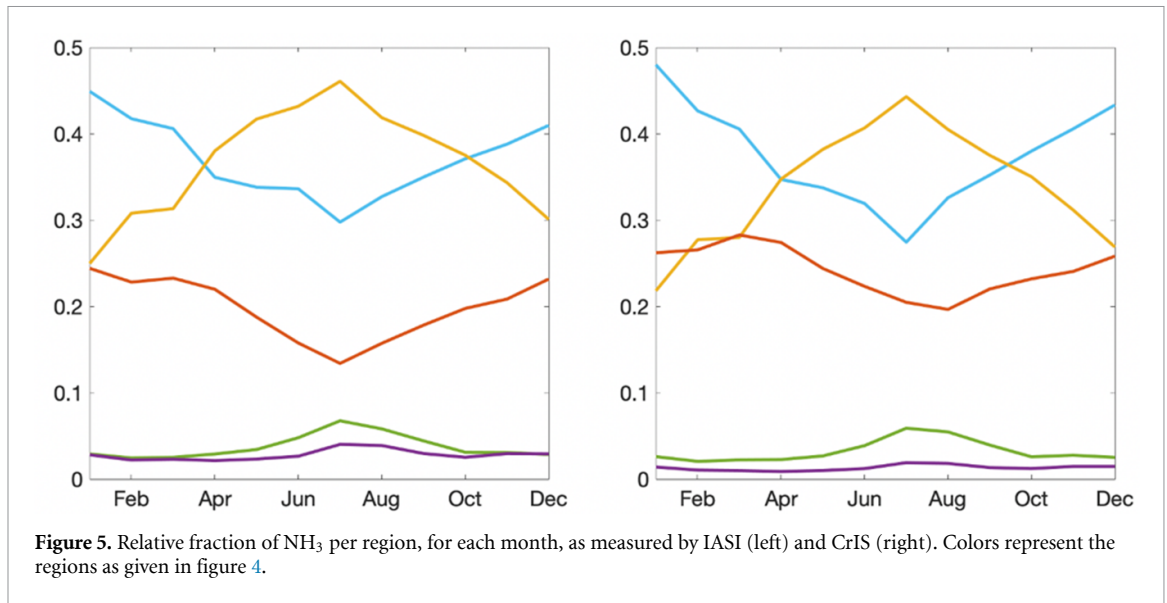
The clustering analysis results in five distinct regions for both IASI and CrIS. The spatial patterns of the clusters are strikingly similar between the two datasets from these independent measurements, demonstrating the robustness with our analysis. The regions with the most distinct seasonality are northwest India and eastern Pakistan (shown in orange and green), and southern and eastern India and Bangladesh (shown in pale blue and red).

Other regions in central and southern India show seasonal variation in observed  $\text{NH}_3$  column density, although the total  $\text{NH}_3$  signal from these areas are relatively low. Seasonal variations in  $\text{NH}_3$  emissions may be present in these areas, however column measurements from satellite are closer to the detection limit. In areas of  $\text{NH}_3$  columns around or below the sensitivity threshold, temporal variations are expected to be difficult to quantify. Figures 4(b)–(d) show the seasonality profiles of each distinct region from IASI and CrIS, respectively. In figure 4(b), the purple and green traces, representing mountainous areas from the Himalaya and Sulaiman Range show

maximum seasonal signal in the mid-summer. These areas however represent a small fraction of total  $\text{NH}_3$  in the study region as shown in figure 5, with between 3% and 6% of total  $\text{NH}_3$  in July coming from these areas. Figure 5 shows significant similarity between the two instruments, with the pale blue sub-region of eastern India dominating  $\text{NH}_3$  columns in December–February and the western IGP (orange) dominating in the mid-summer.

## 5. Discussion

The primary source of  $\text{NH}_3$  in the IGP is from agricultural practices, through volatilization of waste from livestock and nitrogen-based fertilizers for crops. The IGP has two main growing seasons, Rabi (October–March) and Kharif (July–November). Figure 6 shows the seasonalities of  $\text{NH}_3$  column in the western and eastern part of the IGP, along with shaded regions showing the approximate planting dates for the Kharif (June–July) and Rabi (November–February) crops. Most nitrogen-based



fertilizer is applied approximately one month after planting, which agrees very well for the Kharif crop in the western IGP, but no  $\text{NH}_3$  peak is seen for the Rabi season planting dates. High  $\text{NH}_3$  columns in the western IGP during winter have been observed using IASI nighttime (2130) overpasses (Van Damme *et al* 2014), however those data are associated with high uncertainties given the lack of thermal contrast at night. *In situ* measurements in Delhi have also shown high levels of  $\text{NH}_3$  in winter (Sharma *et al* 2010). Fertilizer application is different for rice, with most fertilizers being applied at the time of planting; however, nitrogen-based fertilizer is generally applied 30–90 days after sowing (Craswell *et al* 1981, Singh *et al* 2006, Varinderpal-Singh *et al* 2007). Fertilizer application for rice planted in winter could then explain the  $\text{NH}_3$  peak in April for the eastern IGP, although we do not observe a corresponding  $\text{NH}_3$  peak for the Kharif crop. The eastern part of the IGP

has significantly more rainfall than the western part during the monsoon season (Prakash *et al* 2018), and  $\text{NH}_3$  is known to be scavenged by precipitation events (Black *et al* 1987, Nowak *et al* 2006). This could potentially explain the reduced  $\text{NH}_3$  columns over eastern India and Bangladesh during the monsoon season, while the western IGP maintains relatively higher concentrations.

Biomass burning is also a major source of  $\text{NH}_3$  emissions (Bouwman *et al* 1997). Satellite observations of fire counts from the Moderate Resolution Imaging Spectroradiometer (MODIS) instrument were used to monitor biomass burning in the study region. The majority of fires result from crop-residue and stubble burning in the spring and autumn before replanting.

Figure 7(a) shows the average distribution of biomass burning events during April in the period 2013–2017 from MODIS. There are a large number



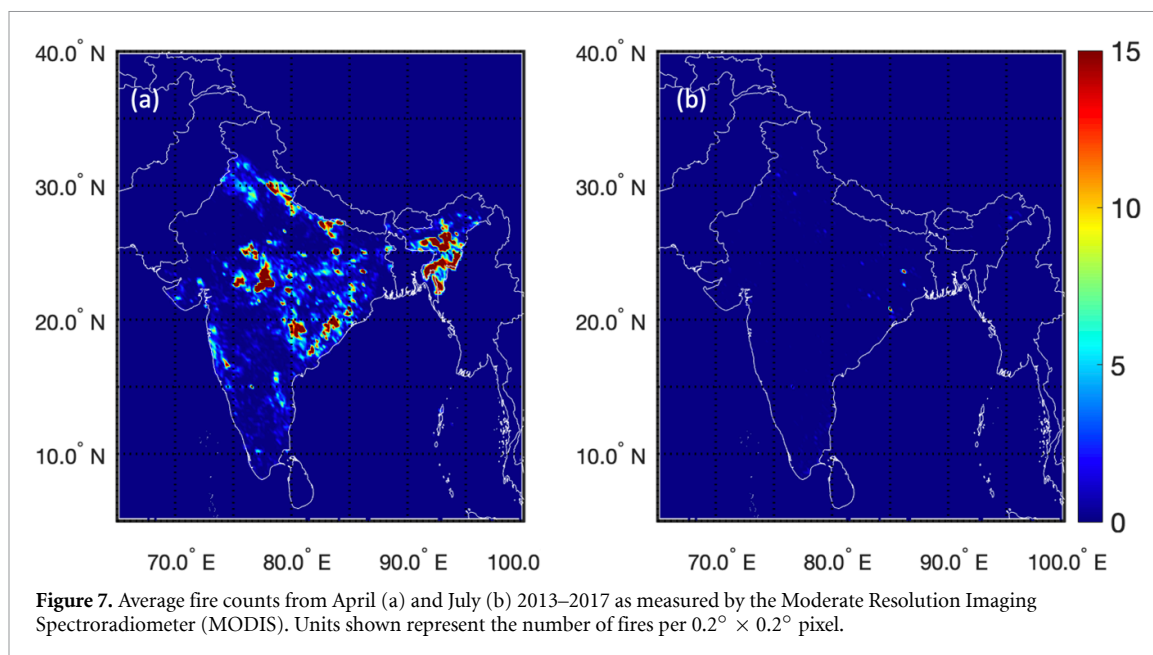


**Figure 7.** Average fire counts from April (a) and July (b) 2013–2017 as measured by the Moderate Resolution Imaging Spectroradiometer (MODIS). Units shown represent the number of fires per  $0.2^\circ \times 0.2^\circ$  pixel.

of fires in Eastern India in this month, which could explain the annual maximum  $\text{NH}_3$  signal seen in this region in figures 4(a)–(c). There are a small number of fires in Northeastern India and very few in Bangladesh. Although these could contribute to the observed  $\text{NH}_3$  columns, it is likely that fertilizer application for rice production is the main cause of the spring seasonal maximum found in this region.

However, maps of fires in India and Pakistan, for example figure 7(b), show no significant biomass burning around the  $\text{NH}_3$  peak in the western IGP in July. It is unlikely that biomass burning, while a significant source of atmospheric  $\text{NH}_3$  in this region (Kuttippurath *et al* 2020), is a major factor in the  $\text{NH}_3$  seasonal peak in July observed in this study.

The satellite  $\text{NH}_3$  seasonal trends show mixed agreement with limited *in-situ* measurements. Kumar *et al* (2004) observed higher  $\text{NH}_3$  in summer than winter at Agra in the IGP, in agreement with the satellite seasonal trends. In Ahmedabad in western India, Sudheer and Rengarajan (2015) showed late June/early July measurements were 10% lower than those in December/early January for a one-year period. IASI/CrIS indeed show a relatively flatter seasonal trend in this region compared to the IGP, yet the satellites have a summer maxima. Sharma *et al* (2010) reported higher  $\text{NH}_3$  in winter than summer and the monsoon months at Delhi, in opposite of satellite trends. More Saraswati *et al* (2018), (2019) measured  $\text{NH}_3$  for five years (2011–2015) in Delhi with a monsoonal minima of 15 ppbv (July–September) and wintertime (November–February) maximum of 25 ppbv. The intrinsic differences between a point-based, surface measurement and column-based satellite measurement may be a key reason for the discrepancy. For example, for the same  $\text{NH}_3$  column, a lower boundary layer in winter will

yield higher surface concentrations than a higher boundary layer of summer, assuming most  $\text{NH}_3$  is in the boundary layer (a reasonable assumption for a surface source and short lifetime species). Indeed, one advantage of column-based  $\text{NH}_3$  measurements is the insensitivity to boundary layer effects which can be difficult to model, especially in winter. India trace gas and  $\text{PM}_{2.5}$  concentrations are strongly impacted by the setup of a strong, shallow boundary layer in winter (Brooks *et al* 2019, Ojha *et al* 2020). Measurements of boundary layer height and vertical profiles of  $\text{NH}_3$  are ultimately needed to compare satellite with surface observations. While more *in-situ* and long-term datasets of  $\text{NH}_3$  are also desired, satellites provide observational  $\text{NH}_3$  constraints for improving air quality studies and emission inventories at monthly and sub-regional scales.

## 6. Implications

The spatial and temporal distribution of  $\text{NH}_3$  total columns have been measured over India, Pakistan and Bangladesh using observations from two separate satellite instruments, the IASI and the CrIS. Using a *k*-means clustering technique, the study region has been divided into sub-regions showing distinct seasonality profiles of  $\text{NH}_3$ . The seasonalities measured by the two separate satellite instruments show the same spatial patterns and temporal evolution throughout the year. These biases are expected to propagate to the simulation of particular matter with implications for air quality and radiative forcing. For instance, Paulot *et al* (2018) showed that distributing CEDS  $\text{NH}_3$  emissions according to the observed seasonality of  $\text{NH}_3$  columns from AIRS (Warner *et al* 2017) reduced the wintertime increase in clear-sky aerosol radiative effect by 30% over the 2002–2015

period. The observations show two main areas of high  $\text{NH}_3$  measurements, the western Indo-Gangetic Plain that has maximum  $\text{NH}_3$  measurements in the mid-summer and the eastern Indo-Gangetic Plain which has maximum  $\text{NH}_3$  in the spring. Across the IGP, there are two main periods of nitrogen fertilizer application, June–July and November–December (Nishina *et al* 2017), corresponding to the Kharif (summer) and Rabi (winter) crops. The observed summer peak of  $\text{NH}_3$  correlates spatially with fertilizer application for the Kharif wheat crop, although there is no corresponding peak seen for the Rabi crop. Ammonia emissions from fertilizer are highly dependent on temperature (Misselbrook *et al* 2004, Xu *et al* 2019) and the IGP has large seasonal temperature changes (Prakash and Norouzi 2020, Narasimha Murthy *et al* 2021), with temperature maxima in late spring and early summer and minima in the winter. The combination of high fertilizer application and temperatures in summer may account for the observed ammonia peak. The spring maximum over eastern India can be explained by the delayed nitrogen-based fertilizer practices (up to 70 days after sowing) for rice production (Latif *et al* 2005, Thind *et al* 2017) and significant fires (figure 7) during this period in eastern-central India. The similarity in spatiotemporal variabilities given by these two independent data sources gives confidence to the patterns described here.

Due to the short lifetime of ammonia, maps of concentrations from satellite should reflect the underlying emissions. The maps shown in figures 1 and 2 are inconsistent with current emissions inventories. This is reflected both on a national scale (figure 3) and significant sub-regional variations (figures 1, 2 and 4). To accurately model ammonia seasonality in India, regionally specific emissions are required. Current emissions models for India use European seasonality data for  $\text{NH}_3$ , a region with different meteorology, relative land use and agricultural practices. This work further shows the large spatial gradients that change monthly in this region.  $\text{NH}_3$  measured from satellite provides an essential check on emissions inventories over this large sub-continent which has diverse emissions sources and sparse surface measurements. In order to disambiguate the multiple emissions sources of  $\text{NH}_3$ , bottom-up measurements are required, particularly during winter in the western IGP.

### Data availability statement

The data that support the findings of this study are available upon reasonable request from the authors.


### Acknowledgments

This work was supported by ExxonMobil through its membership in the Princeton E- filliates Partnership

of the Andlinger Center for Energy and the Environment and by the M.S. Chadha Center for Global India at Princeton University. The authors would like to acknowledge support and data products from the IASI and CrIS satellite science teams. The authors acknowledge support from the NASA Health and Air Quality Applied Sciences team (NASA NNX16AQ90G). X Guo acknowledges the support from NASA Earth and Space Science Fellowship (80NSS-C17K0377). Part of the research at the ULB has been supported by the IASI Flow Prodx arrangement (ESA-BEL-SPO). L Clarisse and M V Damme were supported by the F.R.S.-FNRS.

### ORCID iDs

Rui Wang  <https://orcid.org/0000-0003-0588-1524>

Mark W Shephard  <https://orcid.org/0000-0002-2867-9612>

Mark A Zondlo  <https://orcid.org/0000-0003-2302-9554>

### References

- Acharja P, Ali K, Ghude S D, Sinha V, Sinha B, Kulkarni R, Gultepe I and Rajeevan M N 2022 Global estimates and long-term trends of fine particulate matter concentrations (1998–2018) *Chemosphere* **289** 133155
- Adams P J, Seinfeld J H and Koch D M 1999 Global concentrations of tropospheric sulfate, nitrate, and ammonium aerosol simulated in a general circulation model *J. Geophys. Res.* **104** 13791–823
- Arthur D and Vassilvitskii S 2007 k-means++: the advantages of careful seeding *SODA '07: Proc. 18th Annual ACM-SIAM Symp. on Discrete Algorithms* pp 1027–35
- Awasthi A, Agarwal R, Mittal S K, Singh N, Singh K and Gupta P K 2011 Study of size and mass distribution of particulate matter due to crop residue burning with seasonal variation in rural area of Punjab, India *Environ. Monit. Assess.* **13** 1073–81
- Beer R *et al* 2008 First satellite observations of lower tropospheric ammonia and methanol *Geophys. Res. Lett.* **35** L09801
- Black A S, Sherlock R R and Smith N P 1987 Effect of timing of simulated rainfall on ammonia volatilization from urea, applied to soil of varying moisture content *J. Soil Sci.* **38** 679–87
- Bouwman A F, Lee D S, Asman W A H, Dentener F J, Van Der Hoek K W and Olivier J G J 1997 A global high-resolution emission inventory for ammonia *Glob. Biogeochem. Cycles* **11** 561–87
- Brooks J S A *et al* 2019 Vertical and horizontal distribution of submicron aerosol chemical composition and physical characteristics across northern India during pre-monsoon and monsoon seasons *Atmos. Chem. Phys.* **19** 5615–34
- Clarisse L, Clerbaux C, Dentener F, Hurtmans D and Coheur P-F 2009 Global ammonia distribution derived from infrared satellite observations *Nat. Geosci.* **2** 479–83
- Coheur P-F, Clarisse L, Turquety S, Hurtmans D and Clerbaux C 2009 IASI measurements of reactive trace species in biomass burning plumes *Atmos. Chem. Phys.* **9** 5655–67
- Craswell E T, De Datta S K, Obcemea W N and Hartantyo M 1981 Time and mode of nitrogen fertilizer application to tropical wetland rice *Fertil. Res.* **2** 247–59
- Dammers E *et al* 2016 An evaluation of IASI-NH<sub>3</sub> with ground-based Fourier transform infrared spectroscopy measurements *Atmos. Chem. Phys.* **16** 10351–68

- Dammers E *et al* 2017 Validation of the CrIS fast physical NH<sub>3</sub> retrieval with ground-based FTIR *Atmos. Meas. Tech.* **10** 2645–67
- Felix J D, Elliott E M and Gay D A 2017 Spatial and temporal patterns of nitrogen isotopic composition of ammonia at U.S. ammonia monitoring network sites *Atmos. Environ.* **150** 434–42
- Forgy E W 1965 Cluster analysis of multivariate data: efficiency vs interpretability of classifications *Biometrics* **21** 768–80
- Franco B *et al* 2018 A general framework for global retrievals of trace gases from IASI: application to methanol, formic acid, and PAN *J. Geophys. Res.* **123** 13913–84
- Gilliam J H and Hall E S 2016 *Reference and Equivalent Methods Used to Measure National Ambient Air Quality Standards (NAAQS) Criteria Air Pollutants* vol 1 (<https://doi.org/10.13140/RG.2.1.2423.2563>)
- Gong L *et al* 2013 Role of atmospheric ammonia in particulate matter formation in Houston during summertime *Atmos. Environ.* **77** 893–900
- Guo X *et al* 2021 Validation of IASI satellite ammonia observations at the pixel scale using *in-situ* vertical profiles *J. Geophys. Res.* **126** e2020JD033475
- Hammer M S *et al* 2020 Global estimates and long-term trends of fine particulate matter concentrations (1998–2018) *Environ. Sci. Technol.* **54** 7879–90
- Hellsten S, Dragosits U, Place C J, Dore A J, Tang Y S and Sutton M A 2018 Uncertainties and implications of applying aggregated data for spatial modelling of atmospheric ammonia emissions *Environ. Pollut.* **240** 412–21
- Hoesly R M *et al* 2018 Historical (1750–2014) anthropogenic emissions of reactive gases and aerosols from the community emissions data system (CEDS) *Geosci. Model Dev.* **11** 369–408
- Jain N, Bhatia A and Pathak H 2014 Emission of air pollutants from crop residue burning in India *Aerosol Air Qual. Res.* **14** 422–30
- Kharol S K *et al* 2018 Dry deposition of reactive nitrogen from satellite observations of ammonia and nitrogen dioxide over North America *Geophys. Res. Lett.* **45** 1157–66
- Kotnala G, Sharma S K and Mandal T K 2020 Influence of vehicular emissions (NO, NO<sub>2</sub>, CO and NMHCs) on the mixing ratio of atmospheric ammonia (NH<sub>3</sub>) in Delhi, India *Arch. Environ. Contam. Toxicol.* **78** 79–85
- Kumar A and Sarin M M 2010 Atmospheric water-soluble constituents in fine and coarse mode aerosols from high-altitude site in western India: long-range transport and seasonal variability *Atmos. Environ.* **44** 1245–54
- Kumar R, Gupta A, Kumari K M and Srivastava S S 2004 Simultaneous measurements of SO<sub>2</sub>, NO<sub>2</sub>, HNO<sub>3</sub> and NH<sub>3</sub>: seasonal and spatial variations *Curr. Sci.* **87** 1108e1115 (available at: [www.jstor.org/stable/24108982](http://www.jstor.org/stable/24108982))
- Kuttippurath J *et al* 2020 Record high levels of atmospheric ammonia over India: spatial and temporal analyses *Sci. Total Environ.* **740** 139986
- Latif M A, Islam M R, Ali M Y and Saleque M A 2005 Validation of the system of rice intensification (SRI) in Bangladesh *Field Crops Res.* **93** 281–92
- Leip A *et al* 2015 Impacts of European livestock production: nitrogen, sulphur, phosphorus and greenhouse gas emissions, land-use, water eutrophication and biodiversity *Environ. Res. Lett.* **10** 115004
- Mahapatra P S, Sinha P R, Boopathy R, Das T, Mohanty S, Sahu S C and Gurjar B R 2018 Seasonal progression of atmospheric particulate matter over an urban coastal region in peninsular India: role of local meteorology and long-range transport *Atmos. Res.* **199** 145–58
- Misselbrook T H, Sutton M A and Schofield D 2004 A simple process-based model for estimating ammonia emissions from agricultural land after fertilizer applications *Soil Use Manage.* **20** 365–72
- Mosquera J, Monteny G J and Erisman J W 2005 Overview and assessment of techniques to measure ammonia emissions from animal houses: the case of the Netherlands *Environ. Pollut.* **135** 381–8
- Narasimha Murthy K V, Saravana R, Kishore Kumar G and Vijaya Kumar K 2021 Modelling and forecasting for monthly surface air temperature patterns in India, 1951–2016: structural time series approach *J. Earth Syst. Sci.* **130** 21
- Nishina K, Ito A, Hanasaki N and Hayashi S 2017 Reconstruction of spatially detailed global map of and application in synthetic nitrogen fertilizer *Earth Syst. Sci. Data* **9** 149–62
- Nowak J B *et al* 2006 Analysis of urban gas phase ammonia measurements from the 2002 Atlanta aerosol nucleation and real-time characterization experiment (ANARChE) *J. Geophys. Res.* **111** D17308
- Ojha N, Sharma A, Kumar M, Girach I, Ansari T U, Sharma S K, Singh N, Pozzer A and Gunthe S S 2020 On the widespread enhancement in fine particulate matter across the Indo-Gangetic Plain towards winter *Sci. Rep.* **10** 5862
- Pan Y, Tian S, Liu D, Fang Y, Zhu X, Zhang Q, Zheng B, Michalski G and Wang Y 2016 Fossil fuel combustion-related emissions dominate atmospheric ammonia sources during severe haze episodes: evidence from 15N-stable isotope in size-resolved aerosol ammonium *Environ. Sci. Technol.* **50** 8049–56
- Pant P, Lal R M, Guttikunda S K, Russell A G, Nagpure A S, Ramaswami A and Peltier R E 2019 Monitoring particulate matter in India: recent trends and future outlook *Air Qual. Atmos. Health* **12** 45–58
- Parashar D C, Kulshrestha U C and Sharma C 1998 Anthropogenic emissions of NO<sub>x</sub>, NH<sub>3</sub> and N<sub>2</sub>O in India *Nutr. Cycl. Agroecosyst.* **52** 255–9
- Park J, Kim E, Oh S, Kim H, Kim S, Kim Y P and Song M 2021 Contributions of ammonia to high concentrations of PM<sub>2.5</sub> in an Urban Area *Atmosphere* **12** 1676
- Paulot F, Paynter D, Ginoux P, Naik V and Horowitz L W 2018 Changes in the aerosol direct radiative forcing from 2001 to 2015: observational constraints and regional mechanisms *Atmos. Chem. Phys.* **18** 13265–81
- Pawar P V *et al* 2021 Analysis of atmospheric ammonia over South and East Asia based on the MOZART-4 model and its comparison with satellite and surface observations *Atmos. Chem. Phys.* **21** 6389–409
- Pinder R W, Gilliland A B and Dennis R L 2008 Environmental Impact of atmospheric NH<sub>3</sub> emissions under present and future conditions in the eastern United States *Atmos. Sci.* **35** L12808
- Prakash S, Mitra A K, AghaKouchak A, Liu Z, Norouzi H and Pai D S 2018 A preliminary assessment of GPM-based multi-satellite precipitation estimates over a monsoon dominated region *J. Hydrol.* **556** 865–76
- Prakash S and Norouzi H 2020 Land surface temperature variability across India: a remote sensing satellite perspective *Theor. Appl. Climatol.* **139** 773–84
- Ravishankara A R, Davida L M, Pierce J R and Venkataraman C 2020 Outdoor air pollution in India is not only an urban problem *Proc. Natl Acad. Sci. USA* **117** 28640–4
- Saraswati Y, Sharma S K and Mandal T K 2018 Five-year measurements of ambient ammonia and its relationships with other trace gases at an urban site of Delhi, India *Meteorol. Atmos. Phys.* **130** 241–57
- Saraswati Y, Sharma S K, Saxena M and Mandala T K 2019 Characteristics of gaseous and particulate ammonia and their role in the formation of secondary inorganic particulate matter at Delhi, India *Atmos. Res.* **218** 34–49
- Sharma S K, Datta A, Saud T, Saxena M, Mandal T K, Ahammed Y N and Arya B C 2010 Seasonal variability of ambient NH<sub>3</sub>, NO, NO<sub>2</sub> and SO<sub>2</sub> over Delhi *J. Environ. Sci.* **22** 1023–8
- Sharma S K, Kotnala G and Mandal T K 2020 Spatial variability and sources of atmospheric ammonia in India: a review *Aerosol Sci. Eng.* **4** 1–8
- Shephard M W *et al* 2011 TES ammonia retrieval strategy and global observations of the spatial and seasonal variability of ammonia *Atmos. Chem. Phys.* **11** 10743–63

- Shephard M W *et al* 2020 Ammonia measurements from space with the cross-track infrared sounder: characteristics and applications *Atmos. Chem. Phys.* **20** 2277–302
- Shephard M W and Cady-Pereira K E 2015 Cross-track infrared sounder (CrIS) satellite observations of tropospheric ammonia *Atmos. Meas. Tech.* **8** 1323–36
- Singh B, Gupta R K, Singh Y, Gupta S K, Singh J, Bains J S and Vashishta M 2006 Need-based nitrogen management using leaf color chart in wet direct-seeded rice in Northwestern India *J. New Seeds* **8** 35–47
- Singh N, Murari V, Kumar M, Barman S C and Banerjee T 2017 Fine particulates over South Asia: review and meta-analysis of PM<sub>2.5</sub> source apportionment through receptor model *Environ. Pollut.* **223** 121–36
- Someya Y, Imasu R, Shiomi K and Saitoh N 2020 Atmospheric ammonia retrieval from the TANSO-FTS/GOSAT thermal infrared sounder *Atmos. Meas. Tech.* **13** 309–21
- Sudheer A K and Rengarajan R 2015 Time-resolved inorganic chemical composition of fine aerosol and associated precursor gases over an urban environment in western India: gas-aerosol equilibrium characteristics *Atmos. Environ.* **109** 217–27
- Sun K *et al* 2018 A physics-based approach to oversample multi-satellite, multispecies observations to a common grid *Atmos. Meas. Tech.* **11** 6679–701
- Sutton M A *et al* 2020 Alkaline air: changing perspectives on nitrogen and air pollution in an ammonia-rich world *Phil. Trans. R. Soc. A* **378** 20190315
- Thind H S, Singh Y, Sharma S, Goyal D, Singh V and Singh B 2017 Optimal rate and schedule of nitrogen fertilizer application for enhanced yield and nitrogen use efficiency in dry-seeded rice in north-western India *Arch. Agron. Soil Sci.* **64** 196–207
- Tobin D *et al* 2013 Suomi-NPP CrIS radiometric calibration uncertainty *J. Geophys. Res.* **118** 10510–600
- Van Damme M *et al* 2015 Towards validation of ammonia (NH<sub>3</sub>) measurements from the IASI satellite *Atmos. Meas. Tech.* **8** 1575–91
- Van Damme M *et al* 2021 Global, regional and national trends of atmospheric ammonia derived from a decadal (2008–2018) satellite record *Environ. Res. Lett.* **16** 055017
- Van Damme M, Clarisse L, Heald C L, Hurtmans D, Ngadi Y, Clerbaux C, Dolman A J, Erisman J W and Coheur P F 2014 Global distributions, time series and error characterization of atmospheric ammonia (NH<sub>3</sub>) from IASI satellite observations *Atmos. Chem. Phys.* **14** 2905–22
- Van Damme M, Clarisse L, Whitburn S, Hadji-Lazaro J, Hurtmans D, Clerbaux C and Coheur P-F 2018 Industrial and agricultural ammonia point sources exposed *Nature* **564** 99–103
- Singh V, Singh Y, Singh B, Singh B, Gupta R K, Singh J, Ladha J K and Balasubramanian V 2007 Performance of site-specific nitrogen management for irrigated transplanted rice in northwestern India *Arch. Agron. Soil Sci.* **53** 567–79
- Viatte C *et al* 2020 Atmospheric ammonia variability and link with particulate matter formation: a case study over the Paris area *Atmos. Chem. Phys.* **20** 577–96
- Walker J, Nelson D and Aneja V P 2000 Trends in ammonium concentration in precipitation and atmospheric ammonia emissions at a coastal plain site in North Carolina, U.S.A *Environ. Sci. Technol.* **34** 3527–34
- Wang R *et al* 2021 Monthly patterns of ammonia over the contiguous United States at 2-km resolution *Geophys. Res. Lett.* **48** e2020GL090579
- Warner J X, Wei Z, Strow L L, Dickerson R R and Nowak J B 2017 The global tropospheric ammonia distribution as seen in the 13-year AIRS measurement record *Atmos. Chem. Phys.* **16** 5467–79
- World Health Organization 2016 World Health organization ambient air pollution: a global assessment of exposure and burden of disease *Technical Report* (World Health Organization)
- Xu R, Tian H, Pan S, Prior S A, Feng Y, Batchelor W D, Chen J and Yang J 2019 Global ammonia emissions from synthetic nitrogen fertilizer applications in agricultural systems: empirical and process-based estimates and uncertainty *Glob. Change Biol.* **25** 314–26
- Zavalyov V *et al* 2013 Noise performance of the CrIS instrument *J. Geophys. Res.* **118** 13108–20